Kinematics of a Platform Stabilization using 3-PRS Parallel Manipulator

Tossaporn Udomsap
King Mongkut's University of Technology Thonburi
Sakda Chinchouryrang
King Mongkut's University of Technology Thonburi
Siwat Liampipat
King Mongkut's University of Technology Thonburi
Teeranoot Chanthasopeephan (teeranoot.cha@kmutt.ac.th)
King Mongkut's University of Technology Thonburi https://orcid.org/0000-0001-7437-3705

Research Article

Keywords: 3-PRS Mechanism, Parallel Manipulator, Platform Stabilization

Posted Date: October 24th, 2022

DOI: https://doi.org/10.21203/rs.3.rs-2153038/v1

Kinematics of a Platform Stabilization using 3-PRS Parallel Manipulator

Authors: Tossaporn Udomsap, Sakda Chinchouryrang, Siwat Liampipat, and Teeranoot Chanthasopeephan

Email: tossaporn.udom@gmail.com, sakda7636@gmail.com , paotangban@gmail.com, teeranoot.cha@kmutt.ac.th

Address: King Mongkut's University of Technology Thonburi

126 Prachautit Road, Bangmod, Tungkru, Bangkok 10140

Corresponding author: Teeranoot Chanthasopeephan (email: teeranoot.cha@kmutt.ac.th)

Abstract

In this paper, a 3-PRS (prismatic, revolute, and spherical) parallel manipulator for platform stabilization is designed. The main purpose of this device is to stabilize visual equipment, which is placed on top of a car to inspect electrical transmission cables as part of routine maintenance. Due to the bulky and heavy infrared cameras used during inspections, a stabilizer platform has been designed to handle the weight of camera equipment up to 10 kg. This device consists of two major mechanisms. The first mechanism is able to adjust the angle of the camera. Thus, the user can focus the camera along the electric transmission lines. The second mechanism is for stabilization. The mechanism serves to stabilize the orientation and position of the camera in roll, pitch, and heave directions. To test the performance of the stabilization mechanism, the device is fed with the known value of the angle as regards input. As such, the device is trying to compensate for the change in angle. Results show that errors between input angles and compensated angles are in the range of 0.4-3%. Errors are seen to be within an acceptable range. It is significant that the resultant errors do not affect the orientation of the camera.

Keywords— 3-PRS Mechanism, Parallel Manipulator, Platform Stabilization

I. INTRODUCTION

THIS paper introduces the use of a parallel manipulator for the inspection of electrical transmission cables. As part of routine maintenance, an infrared camera is used to monitor the damage of overheated cables. Without using a stabilization system, the infrared camera takes snapshots of the wires that reverberate and make noises, causing blurry images. Thus, a novel design is proposed: a stabilization platform, which can hold the weight of camera and equipment up to 10kg. The platform is used to stabilize the camera system. The conventional practice for inspecting electric transmission lines is an inspector holding a thermal camera whilst walking along, focusing the camera on the electric transmission lines. This practice requires a large workforce and time. The concept of installing a camera on top of the car is applied to solve the problem. However, it is found that when the vehicle is moving and inspection of the cables is carried out, the quality of the images or the videos that are captured by the camera are of poor quality. Such results are due to the continuous changing orientation of the camera as the vehicle moves along. Hence whenever the vehicle encounters a bump or hole in the road, jittering images and videos are the result. Especially when a thermal camera is used, significant errors can occur. To counteract this, a stabilization model has been suggested, which could remove the effect of vertical motion when the vehicle experiences road bumps [12]. Since the model was developed specifically based on the vehicle's suspension system, this method requires the known parameter of the system for modeling, prior to designing such a

system. Gimbal mechanism is in general used to stabilize a camera system for most autonomous vehicles and UAV[8, 4]. Compare to gimbal car mount and a vibration isolator which are designed to handle camera on the top or the side of a vehicle, can only handle single camera at a time. While dealing with a bigger size system of multiple cameras, it requires a more complicate stabilization approach. The system requires multiple actuators to drive each degree of freedom of the camera holder along with stabilize the system. Heya et al. [7] developed a three degree of freedom electromagnetic actuator to perform image stabilization.

Pulli et al. [1] applied a nonlinear filter to perform real-time video stabilization using a gyroscope. The algorithm used can foil the amount of small motion, rolling shutter distortion as well as smooth out large motion, thus enabling videos to be taken by mobile devices. A variety of methods can be applied to stabilize the images and videos taken [9, 6]. Sensors such as gyroscopes [13] and an inertial measurement unit (IMU) are used for hardware stabilization[15]. Votrubec [14] has introduced a control system for platform stabilization using a gyroscope. Image stabilizer introduced by [10] which applied template matching method with gyrosensors show promising results while reducing oscillation during dynamical motion of a walking robot.

In robotics, parallel manipulators have widely been applied such as industrial robots, space exploration, satellite tracking, and military robots. Advantages of parallel robots over other serial or chain manipulators are that they can handle large loads, have faster response, and are much better in terms of accuracy [3]. Thus, in order to handle a weight of 10 kg, a parallel manipulator is applied to stabilize the camera system. A Stewart platform has been introduced having a six degree-of- freedom (DOF) parallel mechanism, which is highly effective[5]. In some applications, less motion or workspace is required. A modified Stewart platform presents an alternative approach as a reduced DOF parallel manipulator [2]. Having less actuators, the kinematics of a three DOF parallel manipulator is explored [2]. For example, the DELTA robot has three translational motions and is a 3-RPS (revolute-prismatic-spherical) parallel manipulator [11].

In this paper, a parallel robot is designed to stabilize a camera system for an inspection vehicle. A system of multiple camera can be controlled remotely. The stabilizer can be applied on any type of vehicle and a model parameter of the vehicle is then not required. Compensation for travelling over rough terrain is performed by the parallel manipulator.

II. Design

The structure of most camera stabilizers found on the market is serial linkage. However, due to the workload limitation of this chain manipulator, it is more suitable to use a parallel linkage mechanism. A parallel linkage mechanism has a faster response than serial linkage because it has fewer moving parts.

Such a device consists of two main mechanisms. Firstly, the parallel linkage has an angle adjusting mechanism for the platform, which helps the user find focus along the electrical transmission cables. Then, the mechanism hones in on the flip and yaw manipulation. The flip and yaw mechanism has been designed to adjust the camera angle in pitch (θ) and yaw (ϕ) direction,

respectively. The second function of the parallel linkage is to stabilize the platform. The structure of this mechanism is a 3-PRS (prismatic-revolute-spherical) parallel mechanism: originally designed by Carretero et al.,[2]. Primarily, the mechanism serves to stabilize the orientation and the position of the camera in roll (ψ), pitch (θ), and heave (z) direction. In Fig.1, an overview of the design is shown.

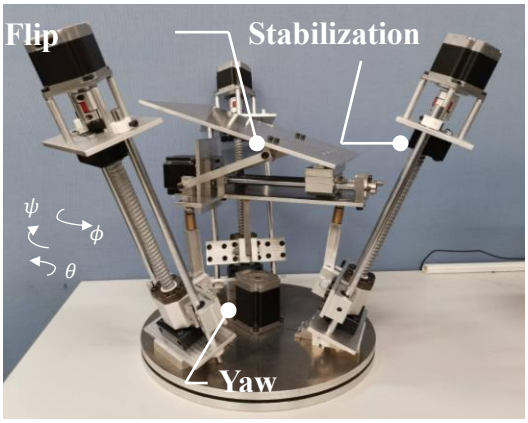

Fig 1. Overview of the device

A. Inverse kinematics

The 3-PRS parallel linkage consists of 3 legs and each leg is identical. The links (each leg) are connected through a prismatic, revolute, and spherical joint. The prismatic joint is an active joint, while the revolute and spherical ones are passive joints. In Fig.2, the vector diagram that represents one leg of 3-PRS is shown. The 3-PRS parallel linkage structure has three degrees of freedom (DOF): namely, roll (ψ), pitch (θ), and heave (z) direction. The 3-DOF is sufficient to stabilize the camera platform, which is placed on top of the vehicle during usage. To manipulate the moving platform of the device so that it can be in the desired orientation or position, an inverse kinematic equation must be obtained.

As shown in Fig. 2, each vector represents:

- $\boldsymbol{P} = [x \quad y \quad z]^T$ is the vector from the origin of base frame
- $\boldsymbol{a_i} = [a_{ix} \quad a_{iy} \quad a_{iz}]^T$ is the vector from origin of moving frame to each attachment point of spherical joint, $\boldsymbol{S_i}$.
- $\boldsymbol{r_i} = [r_{ix} \quad r_{iy} \quad r_{iz}]^T$ is the vector from origin of base frame to $\boldsymbol{S_i}$.
- $\boldsymbol{b_i} = [b_{ix} \quad b_{iy} \quad b_{iz}]^T$ is the vector from the origin of base frame to the origin of moving path of prismatic joint. Note that the magnitude of this vector, $\|\boldsymbol{b_i}\|$ is equal to r_B and constant.

- $\boldsymbol{q_i} = [q_{ix} \quad q_{iy} \quad q_{iz}]^T$ is the vector from the origin of moving path of prismatic joint to each attachment point of revolute joint, $\boldsymbol{R_i}$. Note that the magnitude of this vector, $\|\boldsymbol{q_i}\|$ is equal to the length of each actuator, Q_i which is an acquired value from inverse kinematic equation.
- $\boldsymbol{l_i} = [l_{ix} \quad l_{iy} \quad l_{iz}]^T$ is the vector from $\boldsymbol{R_i}$ to $\boldsymbol{S_i}$. Note that the magnitude of this vector, $\|\boldsymbol{l_i}\|$ is equal to the length of transmitted link, L and constant.

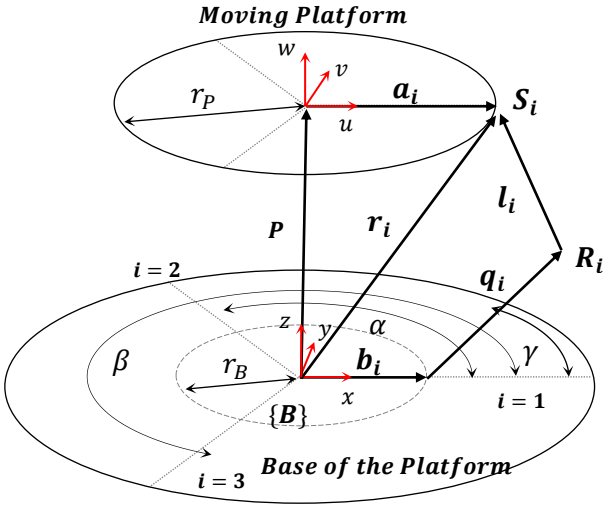

Fig. 2. Vector diagram representing one leg of 3-PRS

The first actuator is placed on the base of the frame. The second and third actuator are placed having α and β angle, respectively, with respect to x-axis. The moving path of each actuator inclines from the horizontal plane having γ angle.

All vectors can be expressed as follows. The vector that is expressed in the moving frame must be converted and expressed as the $\boldsymbol{a_i}$ vector. The $\boldsymbol{a_i}$ vector can be expressed in terms of constant values, as shown below:

$$\boldsymbol{a_1} = [a_{1x} \quad a_{1y} \quad a_{1z}]^T = [r_P \quad 0 \quad 0]^T$$

$$\boldsymbol{a_2} = [a_{2x} \quad a_{2y} \quad a_{2z}]^T = [r_P c_\alpha \quad r_P s_\alpha \quad 0]^T$$

$$\boldsymbol{a_3} = [a_{3x} \quad a_{3y} \quad a_{3z}]^T = [r_P c_\beta \quad r_P s_\beta \quad 0]^T$$

The frame whereby a vector is expressed can be transformed by multiplying the rotation matrix. The rotation matrix that is suitable for the task is Euler's *ZXY* order. Note that c is cos and s is sin:

$$T = R_{y,\theta} R_{x,\psi} R_{z,\phi}$$

$$T = \begin{bmatrix} c_\theta c_\phi + s_\psi s_\theta s_\phi & -c_\theta s_\phi + s_\psi s_\theta c_\phi & c_\psi s_\theta \\ c_\psi s_\phi & c_\psi c_\phi & -s_\psi \\ -s_\theta c_\phi + s_\psi c_\theta s_\phi & s_\theta s_\phi + s_\psi c_\theta c_\phi & c_\psi c_\theta \end{bmatrix}$$

From Fig. 2, the relation from the closed-loop vector chain is obtained:

$$\boldsymbol{r_i} = \boldsymbol{P} + \boldsymbol{T a_i}$$

$$\begin{bmatrix} r_{ix} \\ r_{iy} \\ r_{iz} \end{bmatrix} = \begin{bmatrix} x \\ y \\ z \end{bmatrix} + \begin{bmatrix} T_{11} & T_{12} & T_{13} \\ T_{21} & T_{22} & T_{23} \\ T_{31} & T_{32} & T_{33} \end{bmatrix} \begin{bmatrix} a_{ix} \\ a_{iy} \\ a_{iz} \end{bmatrix}$$

$$\left.\begin{aligned} r_{ix} &= x + T_{11}a_{ix} + T_{12}a_{iy} + T_{13}a_{iz} \\ r_{iy} &= y + T_{21}a_{ix} + T_{22}a_{iy} + T_{23}a_{iz} \\ r_{iz} &= z + T_{31}a_{ix} + T_{32}a_{iy} + T_{33}a_{iz} \end{aligned}\right\} \quad (1)$$

To define the configuration of the structure, the constraint equations are defined. Constraint equations are obtained due to the fact that vectors $\boldsymbol{r_i}$ are only on the same plane as they were. Therefore, constraint equations are shown, for the first, second, and third leg, respectively:

$$r_{1y} = 0 \quad (2)$$

$$r_{2y} = r_{2x}\tan(\alpha) \quad (3)$$

$$r_{3y} = r_{3x}\tan(\beta) \quad (4)$$

Substituting Eqs. (2-4) into Eq. (1) yield Eqs (5-7):

$$y + T_{21}a_{1x} + T_{22}a_{1y} + T_{23}a_{1z} = 0 \quad (5)$$

$$y + T_{21}a_{2x} + T_{22}a_{2y} + T_{23}a_{2z} = \left(x + T_{11}a_{2x} + T_{12}a_{2y} + T_{13}a_{2z}\right)\tan(\alpha) \quad (6)$$

$$y + T_{21}a_{3x} + T_{22}a_{3y} + T_{23}a_{3z} = \left(x + T_{11}a_{3x} + T_{12}a_{3y} + T_{13}a_{3z}\right)\tan(\beta) \quad (7)$$

Substituting vector $\boldsymbol{a_1}$ and rotation matrix T into Eq. (5) yields:

$$y = -c_\psi s_\phi r_p \quad (8)$$

Substituting vector $\boldsymbol{a_2}$, rotation matrix T and Eq. (8) into Eq. (6) gives:

$$x = -\left(c_\theta c_\phi + s_\psi s_\theta s_\phi\right)r_p c_\alpha - (-c_\theta s_\phi + s_\psi s_\theta c_\phi)r_p s_\alpha + \frac{r_p}{\tan(\alpha)}(c_\psi s_\phi(c_\alpha - 1) + c_\psi c_\phi s_\alpha) \quad (9)$$

Substituting vector $\boldsymbol{a_3}$, rotation matrix T, Eq. (8,9) into Eq. (7) yields:

$$\phi = \tan^{-1}\left(\frac{A}{B}\right) \quad (10)$$

where

$$A = \frac{1}{c_\beta}(s_\beta c_\theta c_\beta - s_\beta c_\theta c_\alpha + s_\beta^2 s_\psi s_\theta - s_\beta s_\psi s_\theta s_\alpha + s_\beta c_\alpha c_\psi - c_\psi s_\beta c_\beta)$$

$$B = \frac{1}{s_\alpha c_\beta}(s_\alpha c_\psi c_\beta^2 - s_\alpha c_\beta c_\psi - s_\alpha s_\beta s_\psi s_\theta c_\beta + s_\alpha s_\beta s_\psi s_\theta c_\alpha + s_\alpha s_\beta^2 c_\theta - s_\alpha^2 s_\beta c_\theta - s_\beta c_\psi c_\alpha^2 + s_\beta c_\psi c_\alpha)$$

In Fig. 3, the plane of the moving path of the i-th actuator is shown.

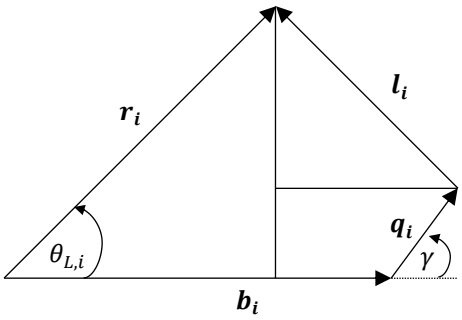

Fig. 3. The plane of moving path of i-th actuator

From Fig. 3, applying the Pythagorean theorem gives:

$$L^2 = \left(r_B - r_i cos\theta_{L,i} + Q_i cos\gamma\right)^2 + \left(r_i sin\theta_{L,i} - Q_i sin\gamma\right)^2 \quad (11)$$

where

$$\theta_{L,i} = \tan^{-1}\left(\frac{r_{iz}}{\sqrt{r_{ix}^2 + r_{iy}^2}}\right)$$

Rewriting Eq. (12) as a function of Q_i yields:

$$Q_i = \frac{-\kappa_i \pm \sqrt{\kappa_i^2 - 4\varepsilon_i \nu_i}}{2\varepsilon_i} \quad (12)$$

where

$$\kappa_i = 2\left(r_B - r_i cos\theta_{L,i}\right)cos\gamma - 2r_i sin\theta_{L,i} sin \quad (13)$$

$$\varepsilon_i = 1 \quad (14)$$

$$\nu_i = \left(r_i sin\theta_{L,i}\right)^2 + \left(r_B - r_i cos\theta_{L,i}\right)^2 - L^2 \quad (15)$$

Hence, the position of the platform is defined via the kinematic equations as defined.

III. Orientation and Position Estimation

In order to stabilize the orientation and position of the camera, the changing orientation and position of the platform's base must

be prior determined. An accelerometer is used to estimate the changes in position while the IMU sensor is used to estimate the change of orientation. A sensor fusion process is applied to both data to enhance its accuracy. The change in orientation and position are substituted into the inverse kinematic equation of the 3-PRS mechanism. Accordingly, the actuators drive the platform to the desired positions. The desired position compensates the change of position in which the base of the platform is altered due to the motion of the vehicle. Eventually, both orientation and position of the moving platform reach the desired position.

A. Orientation estimation by sensor fusion

An accelerometer is used to determine orientation by observing the gravity vector. A gyroscope is used to find the change in orientation via dead reckoning. It is noted, however, that the accelerometer and the gyroscope provide poor quality data, which cannot be directly applied to stabilize the system. For the accelerometer, apart from the gravitational acceleration, it also measures the acceleration, which arises by external forces or movement. If any external forces or movements are detected on any equipment while the sensor is reading, the orientation data is seen to be unreliable. As regards the gyroscope, the process of dead reckoning requires a previous position in order to estimate the current position. Usually, during the sensor reading, noises and biases are presented. Thus, when noises and biases are included in determining orientation, errors accumulate and can affect the calculated orientation. Such a situation eventually causes the orientation to drift over a period.

Sensor fusion can then be set in motion to reduce the undesired effects based on each sensor. The algorithm that is used to fuse the orientation data from the accelerometer and the gyroscope is a complementary filter. The following equations are equations used to find the roll and pitch filtered angle by the IMU sensor:

$$\psi_i = \alpha * (\psi_{i-1} + \dot{\psi}\Delta T) + (1-\alpha) * \tan^{-1}\left(\frac{G_{py}}{G_{pz}}\right) \quad (14)$$

$$\theta_i = \alpha * (\theta_{i-1} + \dot{\theta}\Delta T) + (1-\alpha) * \tan^{-1}\left(\frac{-G_{px}}{\sqrt{G_{py}^2+G_{pz}^2}}\right) \quad (15)$$

where

α weight ratio (range of value between 0-1)

ΔT time step (s)

ψ_i, θ_i roll and pitch angle in current time step, respectively (rad)

ψ_{i-1}, θ_{i-1} roll and pitch angle in previous time step, respectively (rad)

$\dot{\psi}, \dot{\theta}$ rate of change of roll and pitch angle, respectively, acquired from gyroscope(rad/s)

G_{px}, G_{py}, G_{pz} gravitational acceleration in x, y, and z axis, respectively, acquired from accelerometer (m/s^2)

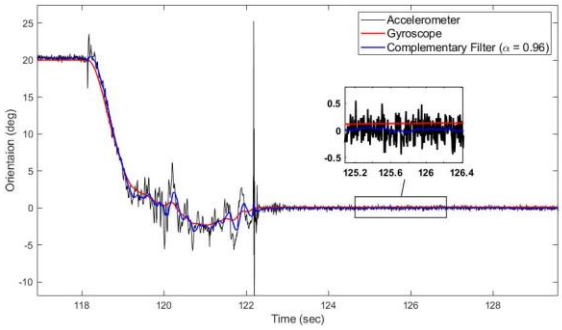

Fig. 4. Orientation data: accelerometer, gyroscope, and complementary filter

Fig. 4 shows that the spiking orientation values from an accelerometer occur when an external force is exerted and the drifting orientation data from the gyroscope materialize over time. The filtered orientation from sensor fusion appears not to be affected by these problems.

B. Position estimation by accelerometer

In this paper, the changing position is acquired by integrating the acceleration data from the accelerometer. Data that has been fed to operate the 3-PRS mechanism must be expressed in an inertial frame while the reading data from the sensor is expressed in a sensor frame, which is moving with the platform. Therefore, multiplying the rotation matrix to transform the coordinate of the data must be performed.

The selected rotation sequence from inertial frame to sensor frame is *ZYX*. Therefore, the rotation sequence from sensor frame to inertial frame is *XYZ*. The rotation matrix from sensor frame to inertial frame in *XYZ* order is:

$$R_B^I = \begin{bmatrix} c_\theta c_\phi & c_\phi s_\theta s_\psi - c_\psi s_\phi & c_\psi c_\phi s_\theta + s_\psi s_\phi \\ c_\theta s_\phi & c_\phi c_\psi + s_\theta s_\phi s_\psi & c_\psi s_\theta s_\phi - c_\phi s_\psi \\ -s_\theta & c_\theta s_\psi & c_\theta c_\psi \end{bmatrix}$$

Acceleration that was integrated to find the changing position must be linear acceleration only (acceleration from movement). Consequently, the gravitational acceleration is compensated:

$$a_I = R_B^I a_m + \begin{bmatrix} 0 \\ 0 \\ g \end{bmatrix}$$

$$\begin{bmatrix} a_{Ix} \\ a_{Iy} \\ a_{Iz} \end{bmatrix} = R_B^I \begin{bmatrix} a_{mx} \\ a_{my} \\ a_{mz} \end{bmatrix} + \begin{bmatrix} 0 \\ 0 \\ g \end{bmatrix}$$

where

a_I acceleration in inertial frame (m/s^2)

a_m acceleration in sensor frame, acquired from accelerometer (m/s^2)

g gravitational acceleration (9.81 m/s^2)

The acceleration in the inertial frame that compensated gravity can be expressed, accordingly:

$$v_i = v_{i-1} + a_{i-1}\Delta T \quad (16)$$

$$p_i = p_{i-1} + v_{i-1}\Delta T \quad (17)$$

where

v_i, p_i velocity and position in current time step, respectively

$a_{i-1}, v_{i-1}, p_{i-1}$ acceleration, velocity, and position in previous time step and inertial frame, respectively

ΔT time step (s)

The position acquired from an accelerometer suffers a similar problem as an orientation and is obtained via a gyroscope. Over time, reading data appears to drift away from true values. In order to solve this problem, an algorithm to define when to start and stop the integration process is presented.

In this paper, a parallel manipulator stabilizes the changing position in the z-axis when a car is passing over road bumps. In Fig.5, the experimental data shows that when the car is passing over road bumps, angular velocity in the lateral axis of the car (y-axis) is spiking. From this information, the threshold of angular velocity in the y-axis is set to categorize the motion of the car and is used to identify whether the car is moving on a normal road surface or passing over a bumpy road. The upper threshold (black dash lines) in Fig. 5 serves as a cut off line.

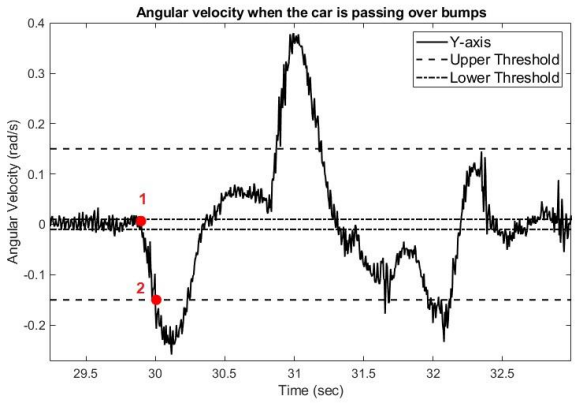

Fig. 5. Angular velocity while car is passing over a bump

If the angular velocity is beyond the upper threshold or the cut offline, integration to determine the change in position is initiated. However, as shown in Eqs. (16) and (17), previous time step terms are required. Fig. 5 shows that point 2 is the point where the algorithm indicates that the car is passing over a bump but the actual starting point is point 1, which means that the previous time-step angular velocity must be found first. The angular velocity of the previous time-step can be found by the following steps. First, when the angular velocity in the y-axis is beyond the upper threshold (point 2), the program will run backwards to find the angular velocity that was in the lower threshold (point 1). Then, the time for point 1 is noted. After that, integration of acceleration is carried out to find the velocity and position from point 1 to point 2. Thus, the value for the velocity and position that resulted from the integration from point 1 to point 2 will be the previous time-step angular velocity.

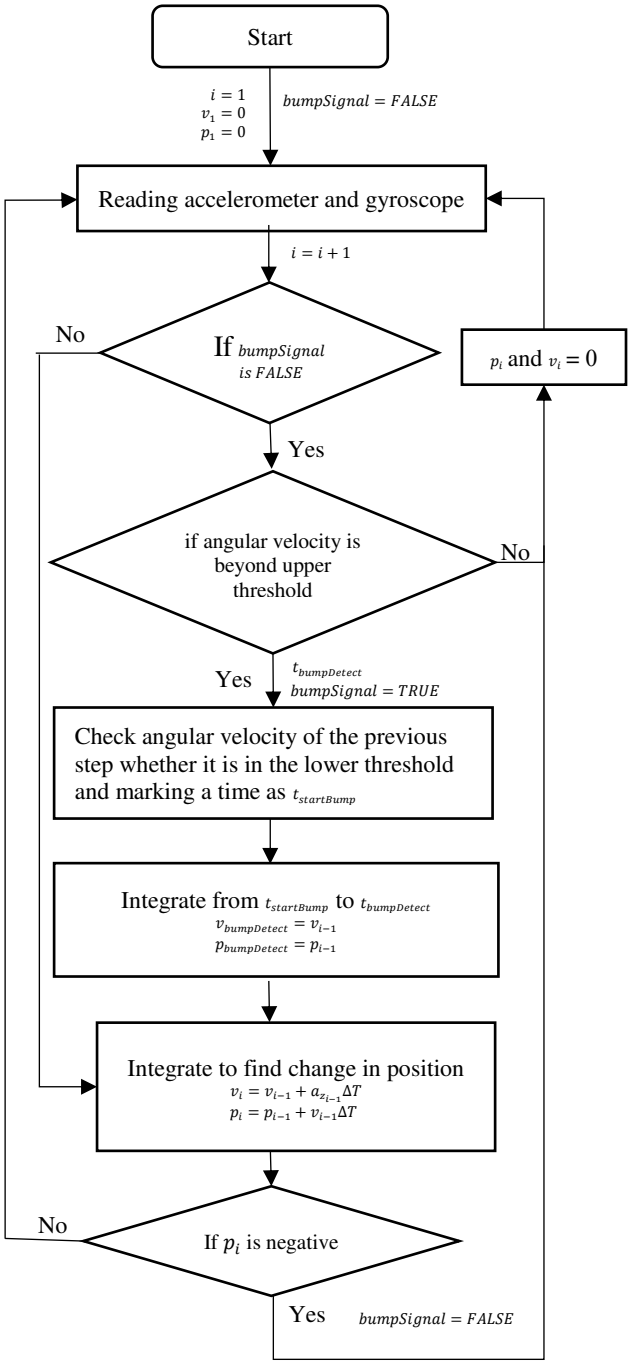

Fig. 6. Flowchart of algorithm for finding changing position via the accelerometer

The flowchart (Fig.6) shows the process used to determine changing of position. Integration from point 2 is continuously carried out until the calculated position has a minus sign. The assumption of an algorithm is that the height of the road before the bump and after the bump are approximately the same. The level of the normal road surface serves as a datum. The sign of height is

positive when above the datum and negative vice versa. The calculated position should never be negative since the device only stabilizes when the car is passing over bumps, excluding the case where the car is passing over potholes.

IV. EXPERIMENT

Two experiments were conducted to test the performance of the stabilization mechanism. In Fig.7, the working process of the stabilization mechanism is shown.

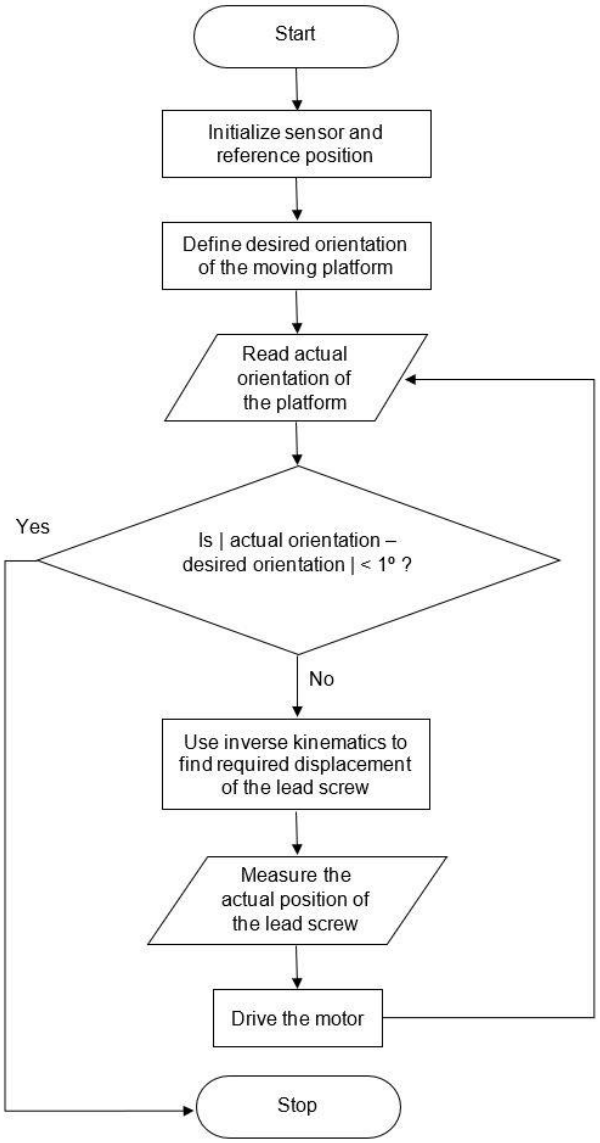

Fig. 7. Flow chart shows the process whereby the stabilization mechanism works to stabilize the camera platform.

A. Feeding the known values of angle as input

For the first experiment, the device was fed with the known values of the angles as input. The angles of the moving platform are measured by the IMU sensor. The measured angles and input were then compared. In Fig. 8, the testing procedure is shown. In Table 1, the results of the measured angles and the input angles are shown.

In Table 1, the errors between input angle and measured angle in the range of 0.4-3% are shown. It is seen that the range of errors was acceptable since the extent of the error did not significantly affect the orientation of the camera. For example, if the orientation of the base platform was changed to 6 degrees, orientation of the moving platform will compensate with 6.18 degrees (as an average result from the experiment). The size of the error, which is 0.18 degree, did not significantly affect the orientation of the camera.

Fig. 8. The device was test with the known angles.

Errors can arise from 2 sources: namely, the friction and clearance of the mechanism and the resolution of the motors. As regards the hardware part, errors are caused through the inaccuracy of measuring the architecture parameters of the 3-PRS structure. For example, vector b_i in Fig. 2 is quite difficult to measure by hand since some parts of the structure present obstacles. As for the resolution of motors, motors are programmed to drive when the difference between actual length and desired length of an actuator is more than 1 millimeter (as shown in Fig. 7). If more resolution is required, this value can be adjusted to be less but should not be too small because the device can pick up more noises instead of real signals.

Input Angle (Deg)	Measured Angle)Deg)					S.D. (Deg)	Mean)Deg)	% Error
	1	2	3	4	5			
2	1.9	1.8	2.2	2.1	2.1	0.15	2.02	1.00
4	4.1	4.0	4.2	4.1	3.8	0.14	4.04	1.00
6	5.7	6.2	6.2	6.4	6.4	0.26	6.18	3.00

8	7.4	8.2	8.3	8.4	8.3	0.37	8.12	1.50
10	9.8	10.1	10	10.2	10.1	0.14	10.04	0.40

Table1. The measured angles as compared to the input angles along with the errors.

B. Testing on the road

For the second experiment, the device was installed on the roof of the car. The camera was attached to the moving platform of the device. While the car is passing over bumps at a constant speed of 10 km/hr, pictures from the camera are captured. In Fig.9, installation of the device on top of the car is shown. In Fig.10, the testing procedure is shown.

In Fig.11, pictures that were captured from the camera are displayed. If the roof of the garage is a reference line, which is the red line in Fig. 11, it shows that the device is somewhat compensating for the change in orientation and position of the camera when the front wheels are passing over bumps, as shown in Fig. 11 (b). However, when the rear wheels pass over bumps, the device stops to compensate for the change in position since the algorithm used to find the changing position halts the integration of acceleration. In section 3.2, it is observed that the integration of acceleration stops when the sign of position is negative. This action shows us that the positions acquired from integration are quite inaccurate. For instance, when the car is passing over bumps, it is impossible that any point of the car will have a negative sign of a position, in other words, below the road surface.

Fig. 9. The installation of the device

Fig. 10. The testing procedure

Fig. 11. Captured pictures from the camera when the car is passing over bumps

The inaccuracy of the changing position that is acquired from an accelerometer is caused by 2 factors. The first factor points out that the acceleration that was integrated is not just linear acceleration because the accelerometer that is attached to the car can be affected by external forces viz. vibration from an engine, vibration from the roughness of a road surface, or an impact between car and bumps. Various forces can affect the accuracy of the calculated change in position.

For the second factor, as seen in Eqs. (16) and (17), the inertial acceleration is a function of the rotation matrix. If the orientation acquired from sensor fusion is not accurate, it can affect the accuracy of the calculated changing orientation.

V. Conclusion

In this paper, a parallel manipulator for platform stabilization was designed and implemented. Experiments were conducted to test the performance of the stabilization mechanism. In the first experiment, known angles were fed to the device as input and the angle of the moving platform was measured. The errors between input angles and platform angles were found to be in the range of 0.4-3%. Errors were caused by the inaccuracy of sensor data, the structural parameters as well as the inaccuracy of the driven motors. It is seen that the camera was attached to the moving platform of the device. The device was installed on top of the car, which was moving at a constant speed of 10 km/hr passing over bumps. The images and videos that were captured from the camera show that the device was able to compensate for the change in orientation and position when the front wheels passed over bumps. However, when the rear wheels passed over bumps, the device came to a stop to compensate for the change in position due to inaccuracy of the calculated changing position. The accuracy of the calculated change in position depends on two main factors. The first factor is that the acceleration, which was integrated to find the position must be linear acceleration only. Any external forces that affect the sensor can contribute to the accuracy of the calculated change in position. The second factor relates to the

accuracy of the orientation, which is also affected by the accuracy of the calculated change in position since inertial acceleration is a function of the rotation matrix.

After testing the device, it shows that there is still room for improvement. The following section presents the possible ways or methods that can improve the performance of the device. The current algorithm used to estimate an orientation is known as a complementary filter. This algorithm suits the static system because orientation acquired from an accelerometer, requires no movement. Such a device, however, becomes dynamic when the vehicle is moving. A Kalman filter, however, may be more suitable for the device because this algorithm has a prediction stage built into the dynamic model and can record measurements from the sensors, which can provide more accurate orientation.

Changing position was estimated by integrating the acceleration that was read from the accelerometer. In order to find the changing position, the acceleration that was integrated must be linear acceleration only. When a sensor is attached to a moving car, many external forces can affect the sensors and influence the accuracy of the calculated changing position. To get rid of or reduce this problem, other types of sensors can be used to improve accuracy. For example, in an autonomous car, an object around the car is visualized by LIDAR sensor. As such, our device can use this principle to visualize a bump or pothole, then predict the changing position that might occur on the device. An alternative method to measure in-progress responses of the moving platform is an optical motion tracker.

Acknowledgements

The authors would like to thank the department of Mechanical Engineering at KMUTT for partial funding support and the use of equipment. This research project is supported by Thailand Science Research and Innovation (TSRI). Basic Research Fund: Fiscal year 2021 under project number 64A306000032.

Author Contribution

All research and experiments are conducted by TU, SC, and SL. TC conducted a research concept, drafted a paper and verify the design and experiment.

Funding

This research project is supported by Thailand Science Research and Innovation (TSRI). Basic Research Fund: Fiscal year 2021 under project number 64A306000032.

Availability of data and materials

Not applicable

Declaration

Competing interests

The authors declare that they have no competing interests.

Author details

Mechanical Engineering Department, King Mongkut's University of Technology Thonburi, Bangkok, Thailand

References

1. Bell, S., A. Troccoli and K. Pulli (2014). A Non-Linear Filter for Gyroscope-Based Video Stabilization. ECCV.

2. Carretero, J. A., R. P. Podhorodeski, M. A. Nahon and C. M. Gosselin (1999). "Kinematic Analysis and Optimization of a New Three Degree-of-Freedom Spatial Parallel Manipulator." Journal of Mechanical Design **122**(1): 17-24.

3. Fatehi, M. H., A. R. Vali, M. Eghtesad, A. A. Fatehi and J. Zarei (2011). Kinematic analysis of 3-PRS parallel robot for using in satellites tracking system. The 2nd International Conference on Control, Instrumentation and Automation.

4. Gašparović, M. and L. Jurjević (2017). "Gimbal Influence on the Stability of Exterior Orientation Parameters of UAV Acquired Images." Sensors (Basel) **17**(2).

5. Gexue, R., L. Qiuhai, H. Ning, N. Rendong and P. Bo (2004). "On vibration control with Stewart parallel mechanism." Mechatronics **14**(1): 1-13.

6. Han, F., L. Xie, Y. Yin, H. Zhang, G. Chen and S. Lu (2021). "Video Stabilization for Camera Shoot in Mobile Devices via Inertial-Visual State Tracking." IEEE Transactions on Mobile Computing **20**: 1714-1729.

7. Heya, A. and K. Hirata (2020). "Experimental Verification of Three-Degree-of-Freedom Electromagnetic Actuator for Image Stabilization." Sensors (Basel, Switzerland) **20**(9): 2485.

8. Jędrasiak, K., D. Bereska and A. Nawrat (2013). The Prototype of Gyro-Stabilized UAV Gimbal for Day-Night Surveillance. Advanced Technologies for Intelligent Systems of National Border Security. A. Nawrat, K. Simek and A. Świerniak. Berlin, Heidelberg, Springer Berlin Heidelberg**:** 107-115.

9. Jia, C. and B. Evans (2013). "3D rotational video stabilization using manifold optimization." 2013 IEEE International Conference on Acoustics, Speech and Signal Processing: 2493-2497.

10. Kurazume, R. and S. Hirose (2000). Development of image stabilization system for remote operation of walking robots. Proceedings 2000 ICRA. Millennium Conference. IEEE International Conference on Robotics and Automation. Symposia Proceedings (Cat. No.00CH37065).

11. Li, Y. and Q. Xu (2007). "Kinematic analysis of a 3-PRS parallel manipulator." Robotics and Computer-Integrated Manufacturing **23**(4): 395-408.

12. Shih, F. Y. and A. Stone (2010). "A New Image Stabilization Model for Vehicle Navigation." Positioning **1**(1): 8-17.

13. Sivčák, M. and J. Škoda (2011). Substitution of Gyroscopic Stabilizer Correction Motor by Active Control of Pneumatic Spring, Dordrecht, Springer Netherlands.

14. Votrubec, R. (2014). "Stabilization of Platform Using Gyroscope." Procedia Engineering **69**: 410-414.

15. Zong, Y.-t., X.-y. Jiang, X.-s. Song, X. Wang and Z.-x. Liu (2010). Design of a two axes stabilization platform for vehicle-borne opto-electronic imaging system. International Conference on Computational Problem-Solving.